J Mater Sci (2023) 58:17154–17174

Ceramics

Control over the mechanical properties of surface-magnetized alumina magnetically freeze-cast scaffolds

Maddie A. Schmitz[1], Isaac Nelson[1], and Steven E. Naleway[1,*]

[1] *Department of Mechanical Engineering, University of Utah, Salt Lake City, USA*

Received: 30 June 2023
Accepted: 31 October 2023
Published online: 23 November 2023

ABSTRACT

Magnetic freeze-casting with a mix of particles and particles of increased aspect ratio (platelets) in surface-magnetized alumina scaffolds gives rise to the Hall effect, which increases the ability to tune scaffold mechanical properties in an unexpected way. Even after surface magnetization, alumina particles are only weakly magnetically susceptible, which has greatly limited their ability to be controlled via Helmholtz coils in magnetic freeze-casting due to their low-strength magnetic fields. The magnetic susceptibility of alumina can be increased by increasing the aspect ratio of alumina particles used. It was found that when a low-strength magnetic field was applied via Helmholtz coils perpendicular to the ice-growth direction to alumina scaffolds at a 1:1 weight ratio of platelets to particles (mixed scaffolds) during freeze-casting, the ultimate compressive strength perpendicular to the applied field and ice-growth direction increased in a statistically significant manner. Lowered viscosity in mixed slurries allowed for more particle movement which resulted in greater Hall voltages than in slurries with a uniform type of particle (either particles or platelets). Using this method, mechanical properties of porous alumina scaffolds can be controlled and tailored to best suit a given application. Given the wide scope of applications of alumina, this method has the potential to be highly impactful for uses ranging from aerospace to dental implants and medical devices.

Handling Editor: Christopher Blanford.

Address correspondence to E-mail: steven.naleway@mech.utah.edu

https://doi.org/10.1007/s10853-023-09108-9

GRAPHICAL ABSTRACT

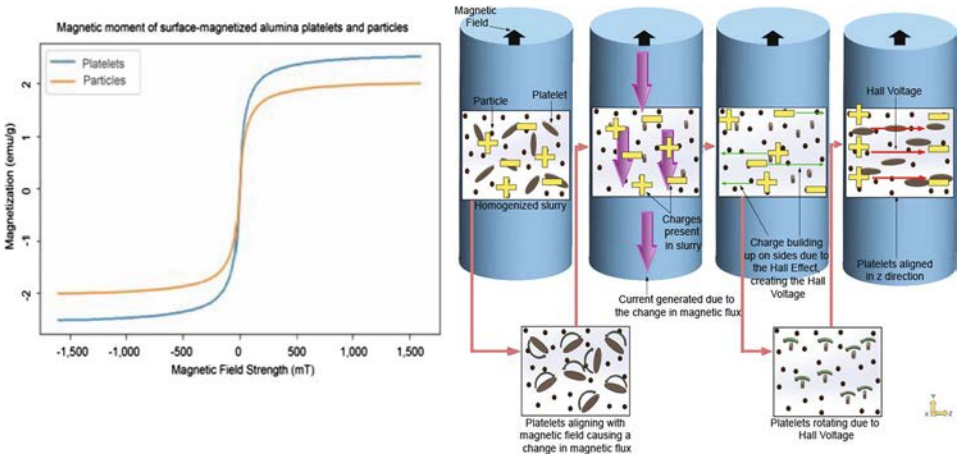

Introduction

Alumina (Al_2O_3) has a number of desirable properties that make it highly attractive for many applications. As the only solid oxide form of aluminum, alumina boasts a high melting point, low thermal conductivity, chemical inertness, and corrosion resistance [1–3]. Additionally, alumina has high permeability which further expands the breadth of its applications [4, 5]. These favorable material properties have made alumina useful in the fabrication of biomaterials such as dental materials (e.g., composites containing such have been used for crowns, dentures) and medical device implants (e.g., hip prosthesis) [1, 6–8]. Additionally, the corrosion resistance and high thermal resistance make alumina promising in the aerospace and automotive fields [9]. As seen in bone, porous materials can be strong and light in weight. Therefore, when creating alumina in a porous configuration, the decrease in weight makes porous alumina even more attractive for the aforementioned applications; though at this point this only holds true in theory. Porous alumina cannot be created at strengths comparable to a solid block of alumina. New techniques, including those inspired by natural materials such as bone, are required to increase the compressive strength of porous alumina to make it better suited for the next generation of ground-breaking technology in the above industries.

One way to create a porous structure that mimics bone is through freeze-casting [10–12]. The freeze-casting process consists of four steps (as diagrammed in Fig. 1a). First, a slurry is created by combining a

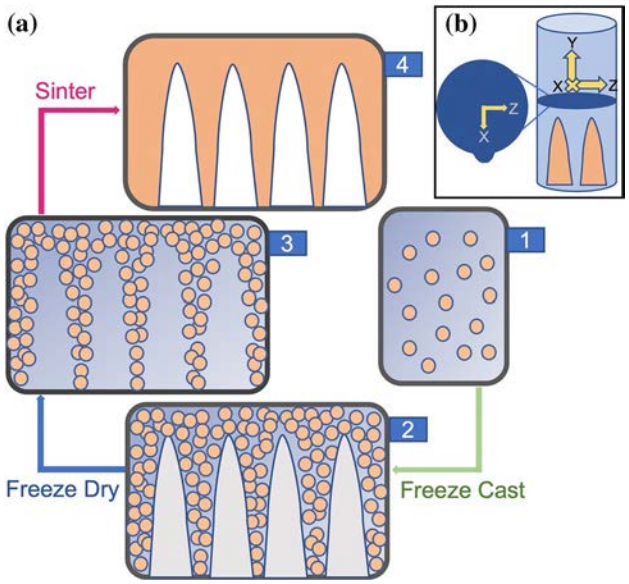

Figure 1 **a** Freeze-casting process consists of the following four steps: (1) A liquid slurry with water, binders, and a solid ceramic are homogenized to create a slurry, (2) the slurry is directionally frozen to form a frozen sample, (3) the frozen sample is freeze-dried to sublimate the ice crystals, which creates a green body that is a rough negative of the ice crystals, (4) the freeze-dried scaffold is sintered to solidify the structure creating a porous material. **b** The coordinate system used in this work is show here on a graphic of a scaffold. Ice crystals are shown growing in the y direction. The magnetic field is applied in the x direction. Scaffolds were created with a notch to in the *x* direction to identify the direction of the applied magnetic field as shown in close up view of the x–z cross section on the left.

liquid freezing agent (water is commonly used), some solid loading (typically a ceramic), dispersants, and polymeric binders. A homogeneous mixture is created by mixing the slurry. Second, the slurry is directionally frozen, causing the ice to grow in a dendritic form. This aligns the solid loading within the slurry, eventually creating the desired porous structure. Changing the freezing rate alters the dendritic structure of the freeze-cast scaffold [13, 14]. Third, the freeze-cast scaffold is sublimated to remove the ice while maintaining the carefully constructed porous structure. A scaffold that has completed sublimation is often referred to as a green scaffold. To complete the process and create a solid porous structure, the fourth step is to sinter the green scaffolds at high temperatures, the result of which is a porous scaffold that resembles the structure of biological materials but falls short in mimicking their properties [10, 15]. Freeze-cast scaffolds are known to have high compressive strengths in the direction of ice growth (y direction in Fig. 1b), but low compressive strengths in directions perpendicular to ice growth (x and z directions in Fig. 1b) [16, 17].

One novel way to remedy this issue while maintaining the strength in the direction of ice growth is to employ the use of energized fields [17–19]. In applying an energized field during the freeze-casting process, it is possible to improve mechanical properties of scaffolds in the directions perpendicular to ice growth by better controlling and aligning the microstructure. Doing so not only improves mechanical properties, but as indicated by Chi et al. aligned scaffolds lead to more ideal arrangements of osteoprogenitor cells and osteoblasts which leads to enhanced biological activity [19]. Electric fields, ultrasound waves, and magnetic fields are just a few of the ways this has been done in the past [11, 19, 21–23]. Magnetic fields have been known to be especially effective in increasing the microstructural alignment, which has resulted in drastic improvements in mechanical properties, with specific reports detailing an increase of 200% in both the modulus and strength of scaffolds [11, 24].

In the past, permanent magnets have been used to magnetically manipulate the microstructure of freeze-cast scaffolds [11, 16, 17, 25, 26]. Altering the orientation and direction of magnetic fields allows for the structure of the target freeze-cast material to be magnetically manipulated. Permanent magnet setups consist of positioning magnets in different positions around the mold of the scaffold while it freezes. High strength fields (120–1320 mT) have been generated by permanent magnets, but at the cost of low uniformity [11, 27]. In freeze-cast scaffolds, non-uniform fields result in particle agglomeration which decreases bulk compressive strength. Due to the nature of permanent magnets and magnetic fields overall, uniform fields are hard to create using permanent magnets [28–32]. It has been found that utilizing a ring setup with permanent magnets to create a rotating magnetic field is effective in to creating a more uniform field for use in freeze-casting [11]. However, such a setup can be complicated to implement and difficult to keep consistent.

Another method of creating a magnetic field is through Helmholtz coils. Helmholtz coils consist of pairs of identical coils connected to one another in series with the distance between them equal to the radius of each coil. A magnetic field is generated when current is run through the coils. The strength of the magnetic field is proportional to the amount of current run through the coils. Previous work has shown that magnetic fields generated by Helmholtz coils used in this study are substantially more uniform than ones produced by permanent magnets [28]. However, Helmholtz coils generate highly uniform fields at the cost of being limited to low field strengths, with previously reported generated field values < 8 mT [34]. As a result, one caveat to utilizing Helmholtz coils-generated magnetic fields to control freeze-cast scaffolds is that the materials used must be highly responsive to a magnetic field (i.e., have a high mass magnetization). Ferrimagnetic materials are ideal due to their high positive magnetic susceptibility [28, 35]. However, utilizing only materials that are ferrimagnetic in nature, such as iron oxide, greatly limits the application of this technique.

To overcome this, alumina can be made magnetically susceptible and able to be magnetically manipulated through surface magnetization [16, 28, 36, 37]. In surface magnetization, materials are coated in superparamagnetic particles and thus become more magnetically susceptible. Superparamagnetic Fe_3O_4 (magnetite) particles are responsive to relatively low-strength magnetic fields (1–10 mT) [36]. These magnetite particles are so small in size (~ 20 nm) that they can be considered a single magnetic domain with one uniform magnetic moment, and therefore respond in a uniform manner when a magnetic field is applied [28]. Ferrofluid can then be created by coating these superparamagnetic particles with a surfactant and conjoining them with a carrier fluid. Coating larger materials with these small superparamagnetic materials is

done using anionic ferrofluid in surface magnetization [17, 28, 35]. Strong electrostatic interactions are created between the opposite charges of the superparamagnetic particles and the larger material particles. Because of this strong bond, non-ferromagnetic materials can be manipulated using a magnetic field. In previous work, Frank et al. [16] showed this by aligning surface-magnetized alumina using a 75 mT field, however, these scaffolds also showed significant agglomeration due to the non-uniform magnetic field generated by the employed permanent magnets. In an attempt to mitigate the issues associated with using permanent magnets, using fields generated by Helmholtz coils to control the structure is highly attractive.

Previous literature has shown that particles with larger aspect ratios have larger magnetic moments. Thus, by using diamagnetic particles of an increased aspect ratio, such as alumina, magnetic moments may be increased to the point of being controllable by a magnetic field, even a low strength magnetic field, such as that produced by Helmholtz coils. In this manuscript, we demonstrate better control over the structure of alumina scaffolds to better mimic the porous structure of bone. By mimicking this structure in freeze-cast scaffolds, we create structures with the positive mechanical properties of alumina while mitigating its low compressive strength to further expand its uses in aerospace, dental implants, and biomedical devices.

Materials and methods

Surface magnetization

Surface magnetization methods were based on previously established methods [17]. Alumina was acquired in each high aspect ratio particles (0.2 μm in minor axis with an aspect ratio of 25:1 here forwards referred to as "platelets," Dreytek Performance Products, Rockaway, NJ) and irregularly shaped/nominally spherical particles (~ 1 μm in effective diameter, here forwards referred to as "particles," Aztron Technologies, Eden Prairie, MN). First, 30 g of alumina (either platelets or particles) were added to 95 mL of tap water and mixed for at least a minute with a glass stir rod to form an alumina solution. Next, 1.2 mL of anionic ferrofluid (Ferrotec (USA) Corporation, Santa Clara, CA) containing 3.9 vol% super-paramagnetic iron oxide nanoparticles (SPIONs) was diluted in 47.4 mL of water to form a diluted ferrofluid solution. The diluted ferrofluid solution was then added to the alumina solution in 10 mL increments per minute. A glass stir rod was used to continually stir the mixture throughout the process. Each mixture was homogenized using a ball mill for 24 h to ensure an even and thorough coating of ferrofluid on the alumina. Upon removal from the ball mill, the water was removed from the mixture by boiling it on a hot plate. The dry alumina was placed in a Buchner funnel on a filter with pores of size 0.22 μm for vacuum filtering. Following the vacuum filtering, a tap water rinse was used to further remove any remaining surfactant from the alumina. Lastly, the alumina was dried at 100 °C for 12 h. After drying, the surface-magnetized alumina was ground using a mortar and pestle to achieve a consistency usable for freeze-casting. The result of this process was approximately 25 g each of surface-magnetized alumina particles and platelets.

Sample preparation

Slurries were created at a volume of 12 mL. The composition of slurries was: 10 vol% surface-magnetized particle or platelet alumina, 1 wt% polyvinyl alcohol (Alfa Aesar, Ward Hill, MA, USA) and 1 wt% polyethylene glycol (Alfa Aesar, Ward Hill, MA, USA) as binders, and 1 wt% Darvan 811 (R. T. Vanderbilt Company, Inc., Norwalk, CT, USA) as a dispersant, along with water as a freezing agent [28, 30, 35]. In mixed scaffolds (described in detail below), 5 vol% was used of each platelets and particles. Slurries were then homogenized via a ball mill for 24 h [17, 32]. Immediately before freeze-casting, slurries were rehomogenized by being sonicated for three minutes at 42 kHz. Following sonication, slurries were poured directly into a PVC mold for freeze-casting. Freeze-casting was performed using a custom freeze-casting apparatus with magnetic fields applied via a custom Helmholtz coils magnetic field setup, as previously described [28, 34]. The magnetic field was applied in the x direction throughout the entire freezing process, and the slurries were frozen directionally at a rate of -10 °C/min beginning from room temperature until the slurry had frozen completely. Once frozen, the ice was sublimated from the samples by freeze-drying at 0.047 mBar at -51 °C for 72 h to create green scaffolds (Labconco, Kansas City, MO, USA). Immediately following sublimation, the green scaffolds were placed into an HTF 1700 open-air furnace (Carbolite Furnaces,

Sheffield, United Kingdom) for sintering at a temperature of 1525 °C for 4 h with a heating and cooling rate of 2 °C/min [15, 24]. The results of this process were fully sintered and stable freeze-cast scaffolds.

Consistent slurry preparation methods were applied throughout the freeze-casting process to investigate the effects of applying a magnetic field to slurries containing different shaped particles. Scaffolds were created with each of the following alumina contents: all platelets (1 platelets: 0 particles, here forwards referred to as "platelet scaffolds"), all particles (0:1, here forwards referred to as "particle scaffolds"), and half platelets, half particles (1:1, here forwards referred to as "mixed scaffolds"). Each of these compositions were created with surface-magnetized alumina, of which an equal number was freeze-cast with a magnetic field applied (7.8 mT) and with no magnetic field applied (0 mT). At least five scaffolds were created under each set of the above conditions for a total of 42 scaffolds.

Mechanical testing

Mechanical testing was performed on scaffolds in the ice-growth direction (y direction), the direction parallel to the applied magnetic field (x direction), and perpendicular to the applied magnetic field (z direction). See Fig. 1b for the visual of the coordinate system. From the middle of each scaffold, 8–12 cubes with cross-sectional areas of approximately 30 mm^2 and heights of 4 mm were created for testing. Four cubes were tested in each the x, y, and z direction to measure the max stress or the UCS (ultimate compressive strength) values. In total, 20 compression tests were performed in each the y, x, and z directions for each combination of field and scaffold type.

Structural analysis

One 2-mm x–z cross-sectional slice was removed from each scaffold for analysis via scanning electron microscopy (SEM). Each cross section was cut in half, creating a semicircle shape, along the x direction to indicate the direction of the magnetic field. SEM images were taken using a FEI Quanta 600FE-ESEM (FEI, Hillsboro, Oregon, USA) at three locations in all semicircle samples at a range of magnifications from 30× to 2000×. For analysis of wall alignment, 100× magnification was used. For all images an accelerating voltage of 7.0 kV and spot size of 6.0 nm was used. Semicircles were coated in 30 nm of gold–palladium prior to imaging.

Data for wall analysis was collected by analyzing images of 100× in ImageJ using methods similar to those previously established [16, 28]. Using ImageJ software (Nation Institute of Health, Bethesda, MD, USA), the areas of distinct wall alignment and the angle at which they occurred were recorded. For each image this was done for all distinct areas of alignment and then each was divided by the total image size to get the alignment in each direction as a percentage of the total image. This procedure was repeated with two semicircle samples taken from four scaffolds of each content type. Alignment data collected above for all combinations of scaffolds was plotted and analyzed to understand the effect of the magnetic field on scaffold microstructure.

Magnetic characterization

Mass magnetization of surface-magnetized particles and platelets was measured using a Microsense FCM-10 vibrating-sample magnetometer (VSM, MicroSense, LLC Lowell, Massachusetts, USA). This was done to characterize how magnetically susceptible particles and platelets were after being surface-magnetized with anionic ferrofluid [28, 35]. The mass of the sample used in each trial was recorded. Then, a sweeping magnetic field (− 1600 to 1600 mT) was applied to a volume (v) of alumina particles or platelets in 200 Oe increments, and the resulting magnetic moment was measured (M, emu). The mass magnetization was then found by dividing the magnetic moment by the recorded sample mass. Three samples each of particles and platelets were run.

TEM and EDS procedures

To further analyze the effect of surface magnetization, transmission electron microscopy (TEM) was used. Images using a transmission electron microscope (TEM) with an accelerating voltage of 15 kV and spot size of 3 nm and energy-dispersive X-ray spectroscopy (EDS) were used to observe how the superparamagnetic Fe_3O_4 particles interacted with the alumina microparticles and perform an elemental analysis, respectively.

Cross-bridge measurement

SEM images of magnification 750× were taken using the procedure outlined in Sect. "Structural analysis" above and were analyzed to quantify the amount of cross-bridging in platelet scaffolds vs particle scaffolds. Three walls from three images of each particle and platelet scaffolds were analyzed. The length of each wall was measured, and the number of cross-bridges coming off each wall was counted. Wall length was then divided by the number of cross-bridges to normalize it per centimeter. Statistical testing was performed on the normalized data using the procedure outlined below in Sect. "Statistical analysis".

Slurry rheology

Two slurries of each variety (platelets, mixed, and particles) of surface-magnetized alumina were created per the procedure laid out in Sect. "Sample preparation" above. Following 24 h of mixing, a Discovery HR20 Hybrid Rheometer (TA Instruments, New Castle, DE) was used to test the viscosity of each type of slurry. Viscosity was measured at room temperature using stainless steel parallel plate attachments. Tests were run for a duration of 60 s with shear rates ranging from 1 to 100 1/S. To ensure homogeneity of the suspension, slurries were sonicated for three minutes immediately before testing.

Measurement of Hall voltage

One surface-magnetized slurry of each content (particles, mixed, platelets) was prepared according to the procedure outlined in Sect. "Sample preparation". All slurries were homogenized via the ball mill for 24 h. Upon removal from the ball mill, each slurry was sonicated as laid out in Sect. "Sample preparation". A slurry was then poured into the PVC freeze-casting mold and exposed to a 7.8mT field generated by the Helmholtz coils in the x direction. The Hall voltage was measured across each direction of the slurry using a digital multimeter (Etekcity, Anaheim, California, USA). After being cleaned via ethanol and let dry, voltmeter probes were inserted with one on each side of the x direction of the slurry to measure the voltage in each corresponding direction and held there until the voltmeter readings stabilized, at which point the voltage was recorded. This was then repeated with one probe located at each the top and bottom of the slurry, and separately with one probe on each side of the z direction of the scaffold to measure the Hall voltage in the y and z directions, respectively. Three Hall voltages were collected in each direction using this procedure.

Statistical analysis

The effect of applying the magnetic field on the UCS in a given direction was analyzed by scaffold contents (platelets, mixed, particles). ANOVA results were further analyzed using a Tukey's honest significant difference (HSD) test. Using Tukey's HSD, UCS of the scaffolds were compared across all directions and content levels. ANOVA and Tukey's HSD were also used to analyze viscosity differences in scaffold type. T tests were employed to analyze the wall alignment measured in scaffolds with and without the magnetic field applied. For all tests, a significance level of $\alpha = 0.05$ was used.

Results and discussion

Surface-magnetized alumina

Magnetism in a material is caused by the movement of electrons within its atoms. The movement of these electrons generate small atomic currents called magnetic dipoles. In materials that are weakly magnetic in nature, equal numbers of electrons spin in each direction throughout the particle to cancel each other out. In materials that are magnetic (ferromagnetic/ferrimagnetic), these currents do not cancel, but rather sum to create a magnetic dipole field for whole particles. When placed in a magnetic field, this net magnetic moment of particles causes them to become aligned in the direction of the field (or opposite depending on the nature of the particle as paramagnetic or diamagnetic, respectively) and thus magnetized. The magnetic dipole moment of a given particle is determined by the sum of the microcurrents within the atoms of the particle and the total particle surface area as seen in Eq. (1). In this experiment, each superparamagnetic Fe_3O_4 particle attached to the surface of the surface-magnetized alumina produces a magnetic dipole. In the TEM images shown in Fig. 2a, the superparamagnetic Fe_3O_4 particles on the surface of

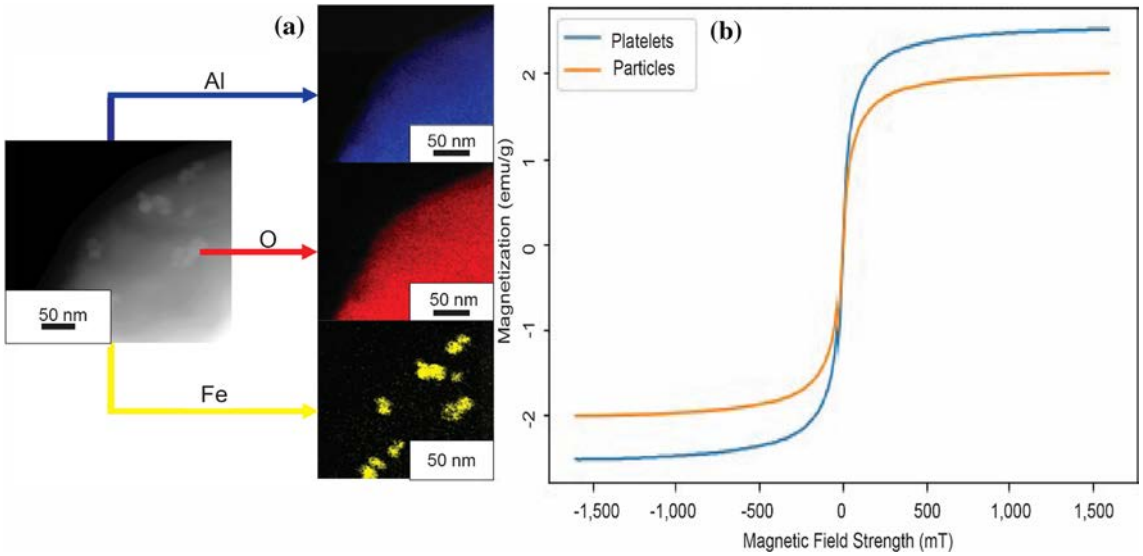

Figure 2 **a** EDS run on TEM images showing location of elements on surface-magnetized alumina particles. **b** Plot of mass magnetization for particles and platelets.

the alumina microparticles can be distinctly identified. As the superparamagnetic Fe_3O_4 particles attach to the surface of the alumina microparticles, the alumina's surface area is directly related to the resultant magnetization. This can be seen in Eq. 1 as particle size is proportional to magnetic moment [38]:

$$\mu = I * A \tag{1}$$

where μ is magnetic moment, I is the net atomic current within the particle, and A is particle surface area. After surface magnetization, the greater surface area of the platelets contains more magnetic dipoles and therefore has a greater magnetic moment. However, even after being surface-magnetized, diamagnetic alumina particles are nowhere near as responsive to a magnetic field as materials that are ferrimagnetic/ferromagnetic in nature [17, 24]. In Fig. 2b, it can be seen that particles have a magnetization value of 2 emu/g, while platelets have a value of 2.5 emu/g. Yet, the 0.5 emu/g increase in magnetization measured in platelets is enough to improve their responsiveness to the small magnetic fields applied in this work.

Platelets vs particles

It has been previously shown that freeze-cast scaffolds composed of non-surface-magnetized alumina platelets have greater UCS values than scaffolds made of non-surface-magnetized alumina particles [39, 40]. In surface-magnetized alumina scaffolds, UCS values were only found to increase in the direction of ice growth when there was no magnetic field present [16]. In addition to the direction of ice growth, experiments performed in this work showed increased UCS values in the cross-section directions (x and z directions) in platelet scaffolds over particle scaffolds (see Fig. 3). This increase in UCS_X and UCS_Z resulted in scaffolds with high UCS values in all three directions (UCS_X, UCS_Y, UCS_Z), rather than just in the direction of ice growth as has been customary in the past with freeze-cast scaffolds [17, 39]. See Fig. 3d for a stress–strain curve illustrating the behavior of platelet and particle scaffolds. This increase in UCS of surface-magnetized platelet scaffold was statistically significant in all three directions regardless of the magnetic field application ($p \leq 0.003$). One additional difference to note between the previous work of Frank et al. [16] and work done here is the size of alumina particles used. This work used 1 μm alumina, while Frank et al. used 350 nm alumina. When using particles that are comparable in size to the platelets, one can better determine the effects of particle aspect ratio on scaffold properties without the effects of different particle sizes. Given the freezing rate used in this work (10 °C min^{-1}) and the size of the platelets, previous literature gives us reason to believe sedimentation should not play a significant role in the freeze-casting of platelet

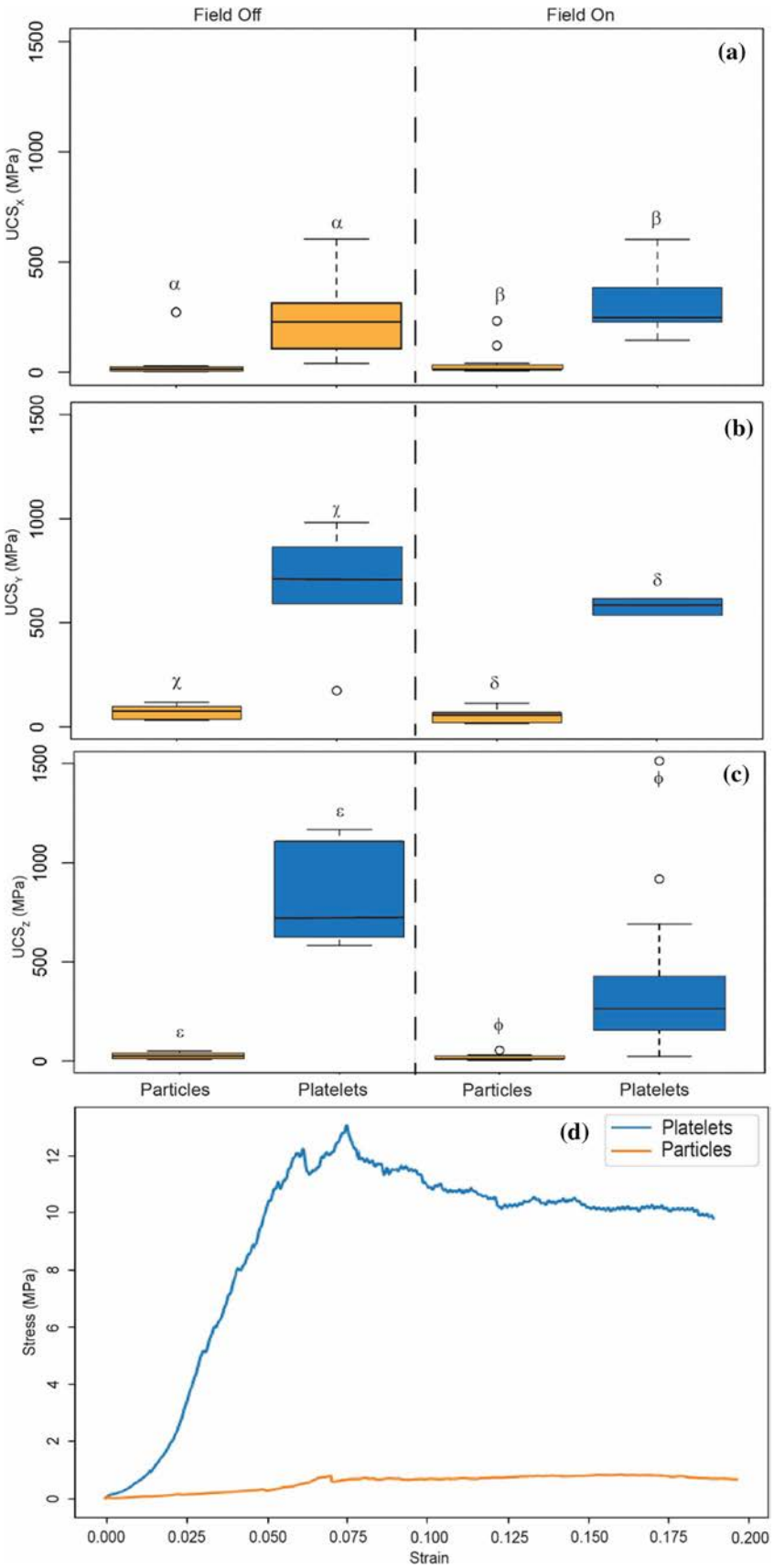

Figure 3 Compressive strength is shown for platelet and particle scaffolds respectively for each direction with and without the magnetic field: **a** UCS_X **b** UCS_Y, **c** UCS_Z. In all cases, platelet scaffolds are significantly stronger than particle scaffolds. Data are presented as a box-and-whisker plot representing the interquartile range with the median value indicated by the line in the middle of the box. The plots are composed of $N \geq 6$ measurements. Statistical significance between samples is indicated by matching Greek letters above the boxes ($p < 0.05$). **d** Representative stress–strain plots are shown for platelets and particles in the x direction with the magnetic field on. Stress in samples would peak once signaling the yield strength and then continue to increase until another peak was reached, the ultimate compressive strength (UCS), before compacting. This trend was characteristic of all scaffolds both when the magnetic field was on and off in all three directions.

scaffolds [41]. Knowing this, we can conclude the scaffold UCS values can be increased in a statistically significant manner by freeze-casting with surface-magnetized alumina platelets in place of alumina particles, which greatly increases the feasibility of creating porous alumina with strength values that more closely resemble those of solid alumina.

Using surface-magnetized alumina platelets in magnetic freeze-casting creates interesting effects within freeze-cast scaffolds allowing for better control of scaffold microstructure. When freeze-casting with just platelets the scaffold microstructure can be controlled by a low-strength magnetic field (7.8mT). When the field is applied the direction of greatest wall alignment is in the direction of the applied magnetic field (x direction). Comparing the microstructure of platelet scaffolds with the magnetic field applied during freeze-casting with those where the field was not applied shows a near statistically significant difference ($p = 0.098$) in wall alignment (see Fig. 4a-c). In particle scaffolds applying the field did not result in clear alignment in any given direction (see Fig. 4d-f).

Unlike in previous work, increased lamellar wall alignment caused by the magnetic field did not result in a statistically significant increase ($p = 0.51$) in UCS of surface-magnetized platelet scaffolds (see Fig. 3). This can be attributed to an increase in cross-bridges in platelet scaffolds caused by platelets packing much less regularly [3, 39, 40]. Figure 5a-c shows the average number of cross-bridges per centimeter in platelet scaffolds, which is greater than that of particle scaffolds by a statistically significant amount ($p < 0.01$). Cross-bridges are the smaller walls that form between lamellar walls usually by particles that are absorbed into the ice crystals as they grow (see illustrations in Fig. 5a-b) [39]. A number of different factors cause platelet scaffolds to have more cross-bridges. First, due to their increased size, the platelets were more likely to split the tip of the ice crystals and become lodged within them forming an increased number of cross-bridges [39, 42]. Secondly, particles of increased aspect ratio are known to rotate around the magnetic field, while their long axis is aligned in the direction of the magnetic field, which can increase cross-bridges or create cross-bridges of greater width. This has been observed in Sendust flakes by Yin et al. [43]. Lastly, interdendritic shear flow is known to cause nacre-like cell wall structures when platelets are used in freeze-casting [3]. All of these factors cause the increased number of cross-bridges seen in platelet scaffolds. In previous literature the increased amounts of cross-bridging occurring when particles of increased aspect ratio are used has resulted in increased UCS in all directions [3, 13, 16, 39, 40]. One instance where the increased wall alignment was accompanied by an increase in strength of the scaffolds was the work of Yin et al. [43]. It is thought that if the experiments performed in this work were to be replicated with these Sendust flakes similar results would be achieved to those seen in this manuscript. Sendust flakes use by Yin et al. were larger in size (10 μm), but of the same aspect ratio. The high magnetic susceptibility of Sendust will cause walls to align, but the larger particle size will lead to lots of cross-bridging which will prevent scaffold UCS from increasing. It is worth noting that differences in sample density properties between the two properties can influence the mechanical properties of samples [44]. Despite the lack of increased strength accompanying the increased alignment, these findings are still significant. This is the first-time freeze-cast microstructure could be controlled in surface-magnetized alumina scaffolds using a low strength magnetic field generated by Helmholtz Coils. Improved microstructural tunability combined with the overall increase in UCS can make surface-magnetized alumina platelet scaffolds an upgrade from particle scaffolds [3, 16, 39]. In doing so, they make platelet scaffolds better suited for bone tissue regeneration, as outlined by Chi et al. [20], and other applications (e.g., dental implants, aerospace, medical devices).

Mixed Scaffolds and the Hall effect

Finding that freeze-casting with surface-magnetized alumina platelets increases the extent to which scaffold microstructure can be magnetically manipulated is of interest. The corresponding increase in UCS seen from freeze-casting with surface-magnetized platelets (compared to that seen in surface-magnetized alumina particles) would be of substantially more interest if it could be controlled to tailor the mechanical properties to best suit any given application. This work attempts to utilize the increased microstructure control of platelets to improve the scaffold mechanical properties in a tailorable manner by employing a mix of platelets and particles, as has previously been shown to be successful [13, 16, 39, 40, 45]. While this has been done previously using permanent magnets, this has never been done using a magnetic field generated by Helmholtz coils. Even when using platelets for only half the solid

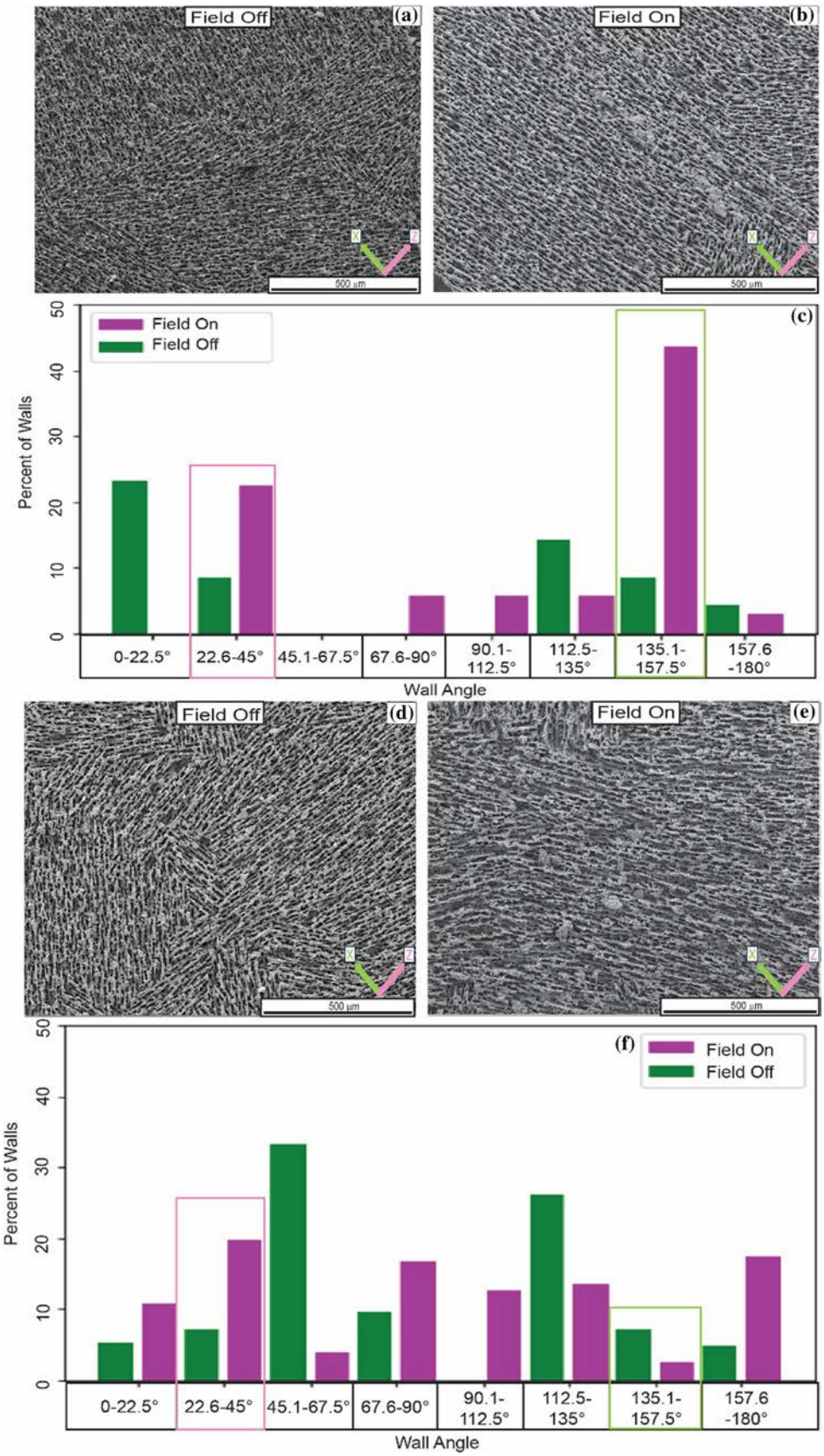

Figure 4 SEM images of **a** platelet scaffolds where no field was applied and **b** where a field was applied in the *x* direction (7.8mT). **c** A high percentage of walls aligned in the *x* direction in **b** are shown in green box in the plot. Scanning electron microscopy (SEM) image of **d** surface-magnetized particle scaffold without the field and **e** with a field applied the *x* direction (7.8mT). **f** Minimal alignment is seen in either the *x* (green box) or the *z* direction (pink box) when the field was applied.

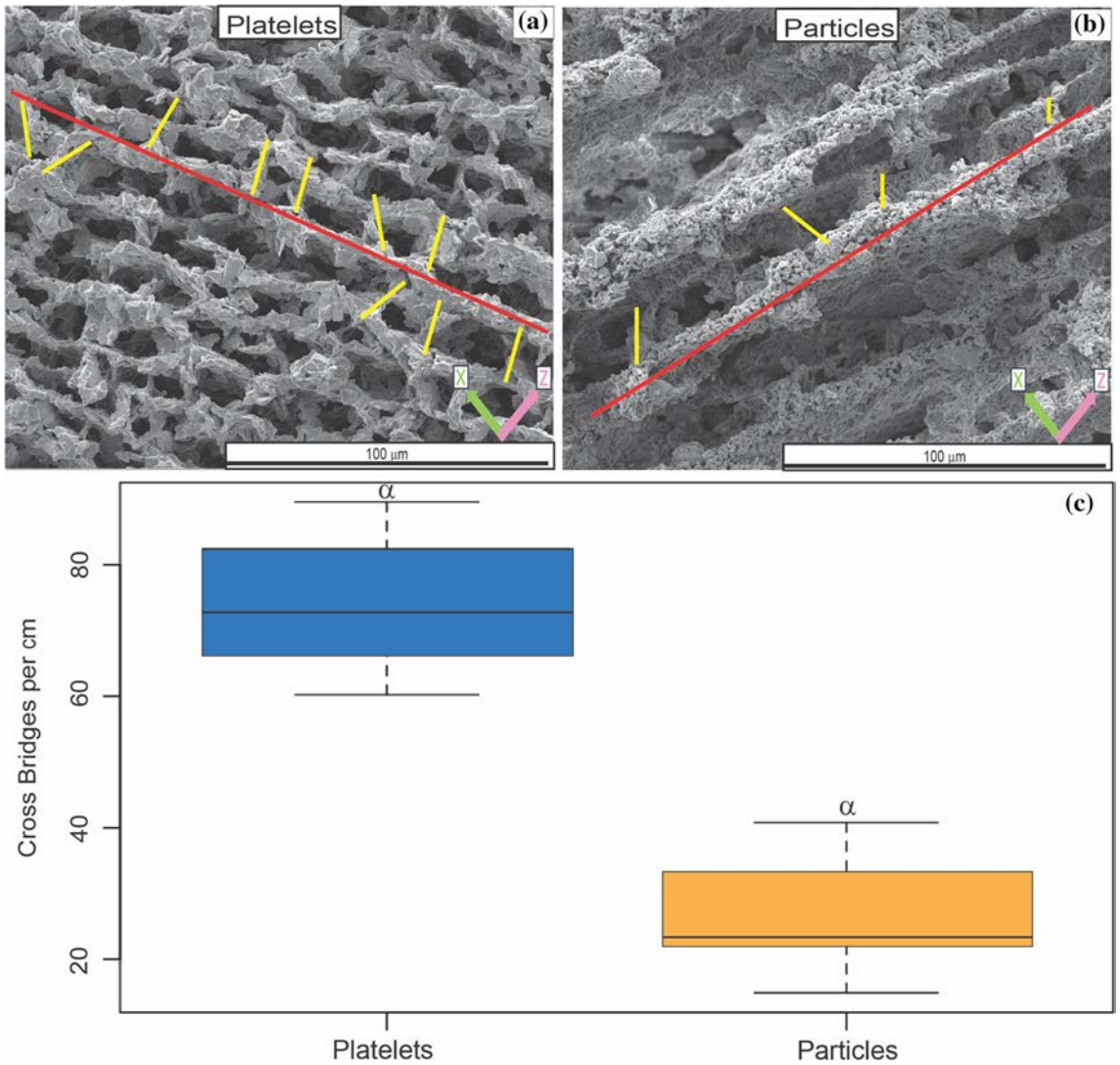

Figure 5 Cross-bridges (in yellow) can be seen branching off of lamellar walls (in red) in the SEM images of **a** a platelet scaffold and **b** a particle scaffold. **c** The number of cross-bridges per centimeter for platelet and particle scaffolds is presented as a box-and-whisker plot representing the interquartile range with the median value indicated by the line in the middle of the box. The plots are composed of $N=9$ measurements. Cross-bridging is greater in platelet scaffolds than in particles by a statistically significant amount, which is indicated between samples by matching Greek letters above the boxes ($p<0.05$).

loading in mixed scaffolds, the increase in magnetization may be significant enough to enable scaffold microstructure control using low-strength magnetic fields. Additionally, it was hypothesized that adding the particles would make mechanical properties easier to control by decreasing the amount of cross-bridging. In doing so, this could make alumina freeze-cast scaffolds with properties tailorable to their uses.

Applying a magnetic field to slurries composed of a one-to-one ratio of surface-magnetized alumina platelets and particles (mixed scaffolds) increased the ability to tune scaffold mechanical properties in an unexpected way. When a magnetic field was applied in the x direction during freeze-casting, the UCS_Z (z = cross-section direction orthogonal to the applied field) of scaffolds increased in a statistically significant manner ($p<0.01$), as shown in Fig. 6. Further increasing the impact of this finding is that previous work was unable to increase UCS values in any direction by applying a much larger magnetic field (75mT) to mixed scaffolds (1:1 ratio) [16]. In this work, now using a magnetic field nearly 10× lower

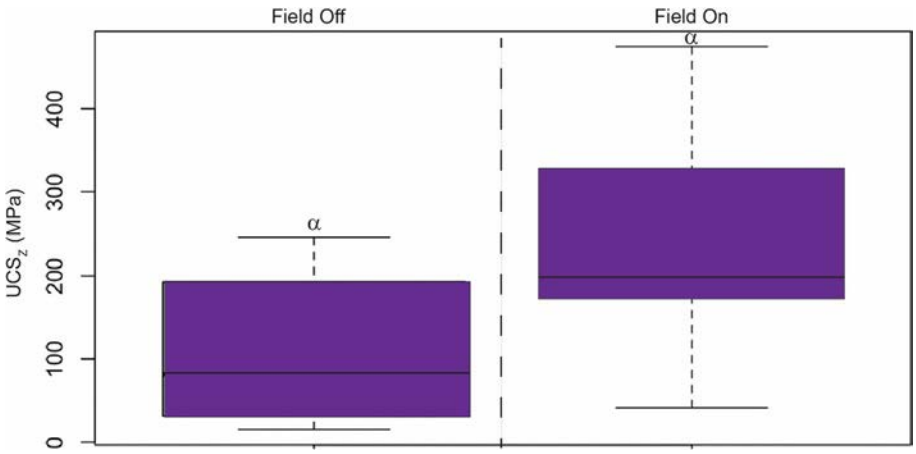

Figure 6 UCS_Z is shown for mixed scaffolds with and without the magnetic field applied. A statistically significant increase in UCS_Z results when the field is on. Data are presented as a box-and-whisker plot representing the interquartile range with the median value indicated by the line in the middle of the box. The plots are composed of $N \geq 28$ measurements. Statistical significance between samples is indicated by matching Greek letters above the boxes ($p < 0.01$).

in magnitude, we are able to do so. Because of this, the resulting scaffolds are no longer transversely isotropic in the plane perpendicular to ice growth (x z plane). In Fig. 7, it is shown that when the field is not applied, UCS_X does not differ in a statistically significant manner from UCS_Z ($p = 0.52$). Though they are not quite statistically significant, it can be seen in Fig. 7 that mixed scaffolds offer UCS_X ($p \leq 0.07$) and UCS_Z ($p \leq 0.05$) values that are greater than those of particle scaffolds when the field is applied. In freeze-cast scaffolds, it is known via previous literature that UCS values in the direction of ice growth (y direction in this work) are far superior to that of the other two directions [11, 46]. This is no longer the case when a magnetic field is applied to surface-magnetized mixed scaffolds. The increase in strength in the z direction in surface-magnetized mixed scaffolds caused by the application of a magnetic field makes the UCS_Z comparable to that of UCS_Y (see Fig. 8). Previously, this lack of strength in the directions perpendicular to ice growth has limited the applications of freeze-cast scaffolds. Thus, the breadth of potential applications for mixed scaffolds is greatly expanded since this is no longer the case.

This increased level of tunability in the direction perpendicular to the direction of the applied field is caused by the Hall effect [47]. When electric current flows through a conductor in a magnetic field, charge carriers (e.g., the surface-magnetized alumina platelets and particles) are subject to a transverse force that is associated with the Hall effect. The voltage in the slurry inducing the current is caused by the changing magnetic flux caused by the movement of conductors (e.g., platelets rotating to align) in the presence of a magnetic field, known via Faraday's Law, which is shown in Eq. 2:

$$\varepsilon = \frac{-d\Phi_B}{dt} \tag{2}$$

where $-d\Phi_B$ is the change in magnetic flux, dt is the change in time, and ε is the electromotive force or the electromotive voltage. Figure 9a shows the magnetic field (black arrow) being applied to a freshly homogenized slurry. Figure 9b shows the platelets aligning with the applied magnetic field, causing a magnetic flux. The change in magnetic flux induces a voltage in the slurry. Free charges present in the slurry then flow across this potential difference. In Fig. 9c, this current is represented by the purple arrows. The current induces the Hall effect within the slurries which causes the alignment of the walls in the z direction seen in mixed scaffolds. As current flows, its charges are deflected by the magnetic field with positive charges being drawn to one side of the slurry, while negative charges are drawn to the other. In Fig. 9d, this buildup of charges can be seen by the yellow plus signs being pulled to one side of the slurry and the yellow minus signs to the other. This continues until the force, F, caused by the charge buildup,

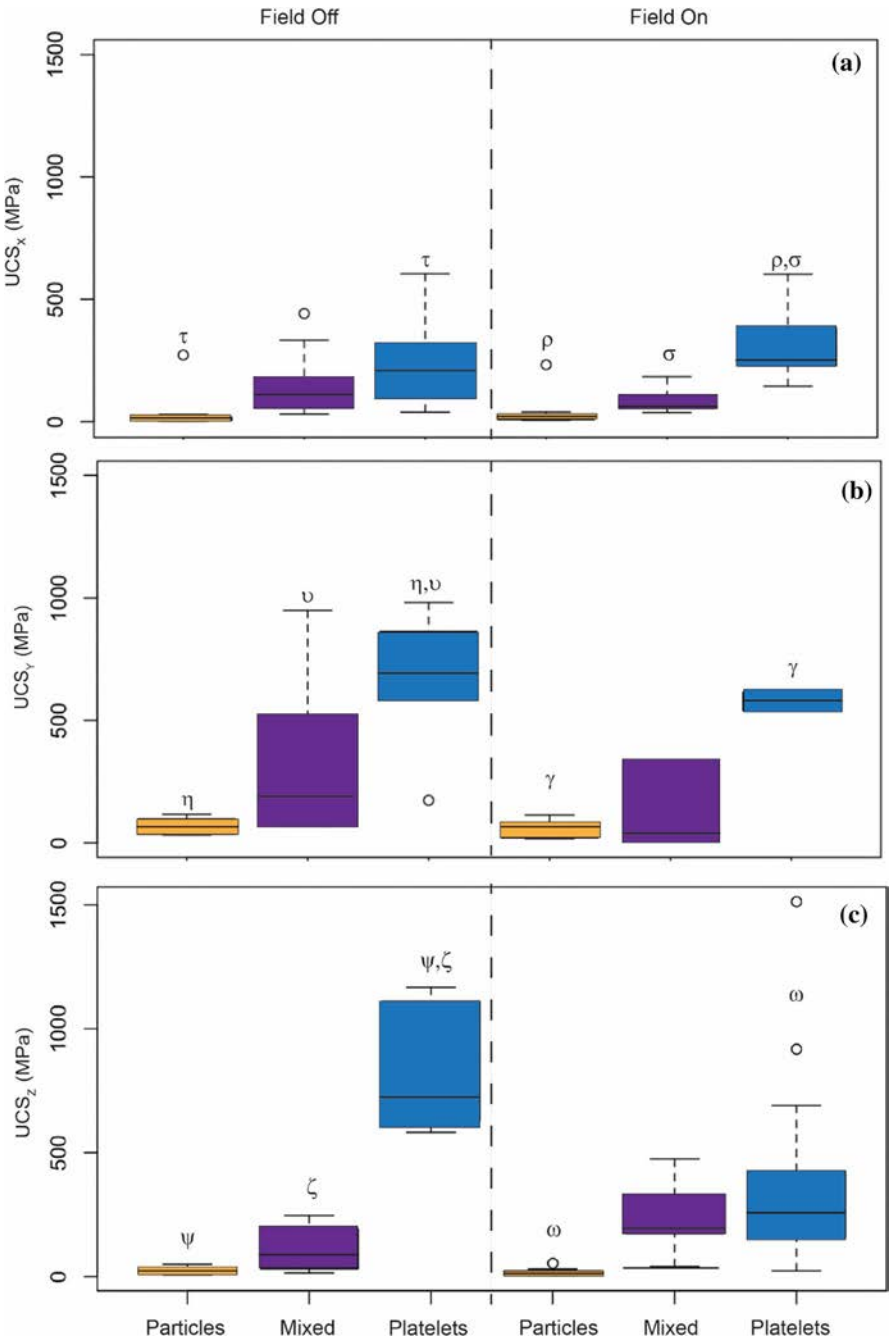

Figure 7 Compressive strength is shown for mixed scaffolds with those of platelet and particle scaffolds for each direction with and without the magnetic field: **(a)** UCS_X, **(b)** UCS_Y, and **(c)** UCS_Z. Without the field applied mixed scaffolds are consistently stronger than particle scaffolds and, in some instances, as strong as platelet scaffolds. Data are presented as a box-and-whisker plot representing the interquartile range with the median value indicated by the line in the middle of the box. The plots are composed of $N \geq 11$ measurements. Statistical significance between samples is indicated by matching Greek letters above the boxes ($p < 0.05$).

$$F_z = |q|E_e = |q|Vd \tag{3}$$

is equal and opposite in force to that of the magnetic field,

$$F_z = qv_{dy}x\,B_x = |q|\,v_{dy}B_x \tag{4}$$

where q is the magnitude of a charge, E_e is the value of the electric field, V is the Hall voltage, d is the distance over which the drop occurs (the width of the slurry), v_{dy} is the drift velocity of moving charges, and B_x is the magnitude of the applied magnetic field [38]. At this point, no more charges flow to either side, but a voltage remains due to the charges that have built up (the Hall Voltage) as seen in Fig. 9d According to Young et al. [38], Eq. 4 can be used to calculate the magnitude of force in the z direction due to the Hall voltage. Platelets within the slurry are then aligned by this Hall voltage in the direction perpendicular to

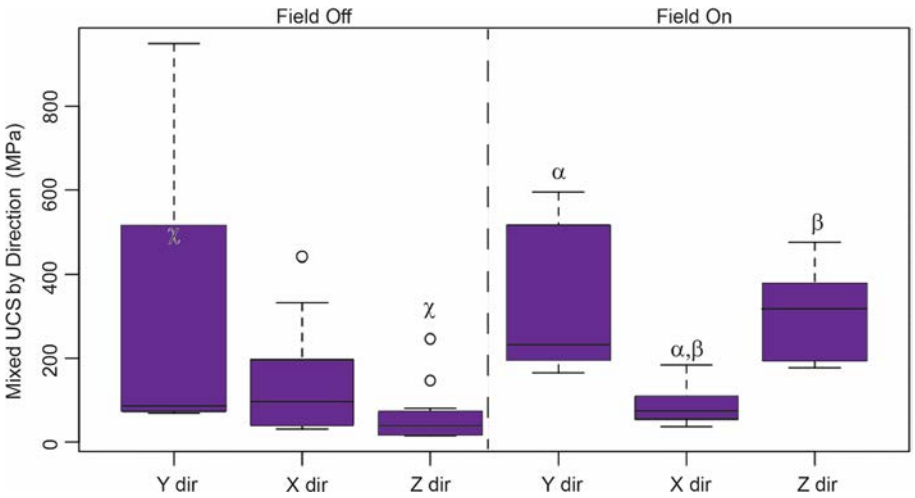

Figure 8 UCS_X, UCS_Y, and UCS_Z with and without the applied field are shown for mixed scaffolds. Applying the magnetic field results in a statistically significant increase in UCS_Z making it comparable in UCS_Y. Data are presented as a box-and-whisker plot representing the interquartile range with the median value indicated by the line in the middle of the box. The plots are composed of $N \geq 28$ measurements. Statistical significance between samples is indicated by matching Greek letters above the boxes ($p < 0.05$).

the magnetic field, as shown in Fig. 9e. To confirm this, the Hall voltage was measured in slurries as the magnetic field was applied. In the z direction, a Hall voltage of 12 mV was measured for mixed scaffolds. A much lower voltage of 3 mV was measured across the x direction. Thus, it is confirmed that the Hall effect is responsible for increase in strength seen in the z direction of mixed scaffolds. Using this knowledge, it can be confirmed via Eq. 4 that the direction of drift velocity, v_d, and therefore the current, is in the y direction. Drift velocity is the speed with which charged particles move in the presence of an electric field or voltage and determines the current

$$I = v_d neA \tag{5}$$

where I is the current flow, n is the free electron density, e is the charge of an electron, and A is the cross-sectional area over which the current flows. In other words, Eq. 5 shows that the direction of current flow is determined by the drift velocity. Knowing the direction of the measured Hall voltage and the applied magnetic field, it can be seen from Eq. 4 that the direction of current flow chosen in Fig. 9 is validated. The result of calculating the cross-product of the applied magnetic field (x direction) with the drift velocity must result in a Hall voltage in the z direction. Thus, for this to be the case, the drift velocity (current) must occur in the positive or negative y direction as shown in Fig. 9c. The current has been shown in the positive y direction, but the sign is of little significance as either will result in a Hall voltage in the z direction as observed. Voltages measured in platelet slurries when checking for evidence of the Hall effect via Hall voltages were significantly smaller at a value of 3–5 mV. Using Eq. 3, it can be seen that the force caused by the Hall voltage of mixed scaffolds is 3× greater than that of the platelet scaffolds:

$$F_z = |q|Vd = (4mV)\,|q|d \quad \text{(for platelet scaffolds)}$$
$$F_z = |q|Vd = (12mV)\,|q|d \quad \text{(for mixed scaffolds)}$$

In platelet scaffolds, the force resulting from the Hall voltage is three times less than in mixed scaffolds, and thus the walls remain aligned in the x direction with the magnetic field in platelet scaffolds (as previously seen in Fig. 4a-c).

Combining surface-magnetized alumina platelets and particles in mixed slurries creates slurries of lower viscosity than when only one particle size is used, which enables control of the material properties via the Hall effect (see Fig. 10 for slurry viscosities). Via previous literature, it is known that suspensions containing multiple particle sizes have lower viscosity than those containing just one size particle [48]. In a suspension containing particles of all the same size, movement is impeded by the particles getting caught

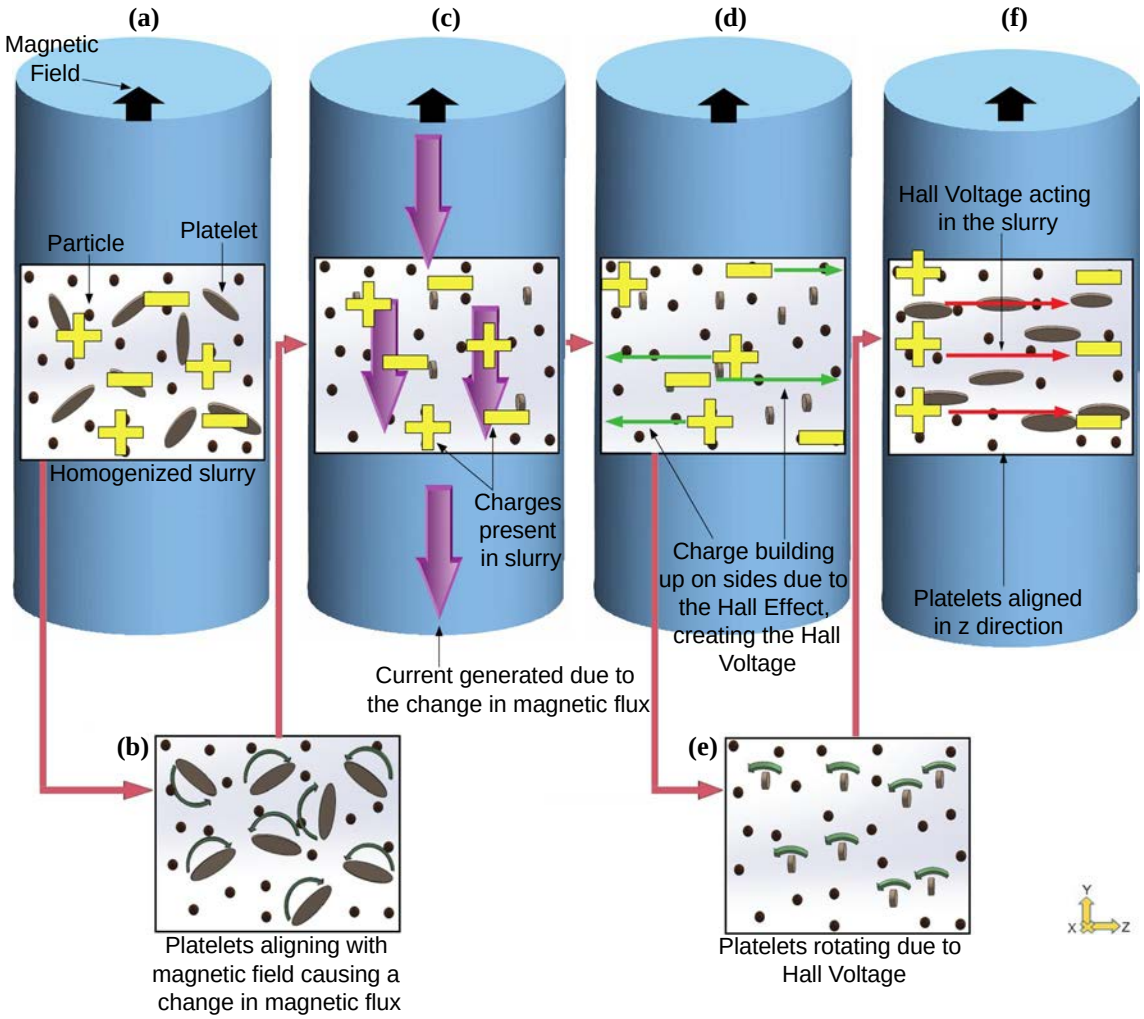

Figure 9 Hall effect as seen in mixed scaffolds is shown here. **a** A freshly homogenized slurry in which the particles and platelets are oriented in randomly. **b** Platelets move to align themselves with the magnetic field applied in the *x* direction (shown with a black arrow at the top of the scaffold). **c** The movement of these charge carriers causes a change in magnetic flux in the slurry, which generates a current across the slurry. **d** The electric current generated causes charges to build up on the sides of the scaffold (see yellow pluses and minuses). **e** This charge buildup causes a measurable Hall voltage across the scaffold with which the platelets become aligned **f**. This alignment results in alignment of the structure and the increase in UCS_Z of mixed scaffolds when the magnetic field is applied.

on one another. When particles of different sizes are used, less collisions occur, and particles move more freely throughout the suspension as a result [48]. Due to this, platelets are not able to align with the magnetic field as quickly in platelet scaffolds, which results in a smaller magnetic flux and thus a smaller current in the scaffold. Smaller current values prevent charge buildups within the slurry from getting large enough to have a force that is equal and opposite to that of the magnetic field.

The direction of maximum wall alignment in mixed scaffolds is neither the direction of the field applied nor the direction of the Hall voltage. Instead, the directions of most alignment falls between the two directions with the greatest being in the middle. In previous literature, the walls are most aligned in the direction of greatest strength within the scaffold [16, 24, 33]. Based on mechanical testing results discussed above, the expected direction of greatest alignment would be in the *z* direction. The above explanation of how the inner-workings of the Hall

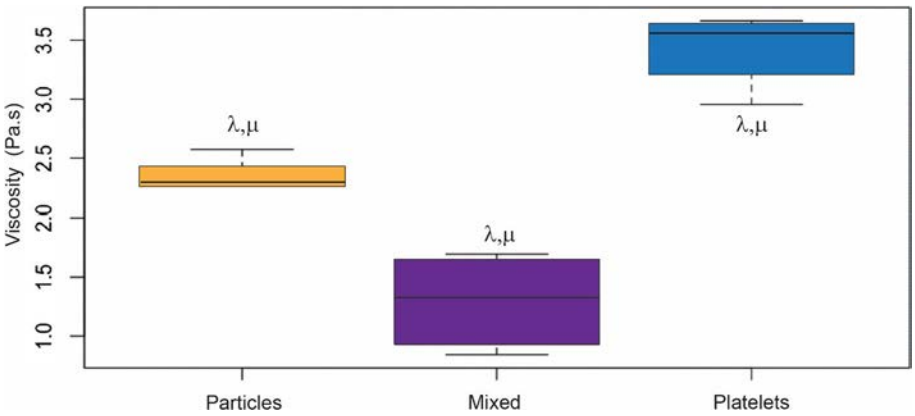

Figure 10 Viscosity is shown for all three types of slurries: particles, mixed, and platelets. Mixed slurries were less viscous than both particle and platelet scaffolds. Data are presented as a box-and-whisker plot representing the interquartile range with the median value indicated by the line in the middle of the box. The plots are composed of $N=3$ measurements. Statistical significance between samples is indicated by matching Greek letters above the boxes ($p<0.05$) .

voltage explains this behavior. Until enough charge has accumulated on the sides of the slurry, the force due to the magnetic field is greater than that of the Hall voltage [38]. Therefore, we can assume the platelets are mostly aligned with the magnetic field. Once enough charge has accumulated that the force from the Hall voltage is equal to that of the magnetic field, the force acting on platelets is in the z direction due to Hall effect. This causes the alignment in the scaffold to transition from the x direction to the z direction.

Meanwhile, the ice crystals have grown resulting in the remaining slurry contents being concentrated. Because of this, platelets are more likely to become caught on one another which prevents walls from becoming most aligned in the z direction [49]. This can be seen in Fig. 11b where the directions of greatest wall alignment fall between the x and z directions. There is an increase in wall alignment in the z direction (nearly double the percentage of total walls) when the field is applied, but more often the platelets become caught in their transition from the x direction to the z. The combination of increased alignment in the z direction with the walls aligned between the x and z direction altered the microstructure of the scaffold sufficiently to result in a statistically significant increase in UCS_Z seen in mixed scaffolds.

These findings of the Hall effect being present in mixed scaffolds is highly impactful in a number of ways. Previously, the Hall effect has been used in various types of sensors and to measure/predict flow rate in liquids [50–52]. Not only is this work the first time the Hall effect has been used to control a particles within a colloidal slurry, it is also the first time it has been seen in freeze-cast scaffolds/slurries. This opens the door for future experiments to learn more about the properties of freeze-cast slurries by way of the Hall effect to further increase tunability of freeze-cast scaffolds. Using the Hall effect in this work enabled control of the previously uncontrollable mechanical properties of freeze-cast alumina scaffolds. Even more impressive is that this level of control was unable to be achieved in alumina freeze-cast scaffolds of a 1:1 ratio of platelets to particles using permanent magnets 10 × greater in strength. This increased level of mechanical property tunability and the UCS values that accompany make the findings of this work novel and take porous alumina freeze-cast scaffolds steps closer to being implementable in the aerospace and biomedical fields. One now can use a low-cost, easily implementable Helmholtz coils setup to tailor mechanical properties of porous alumina scaffolds.

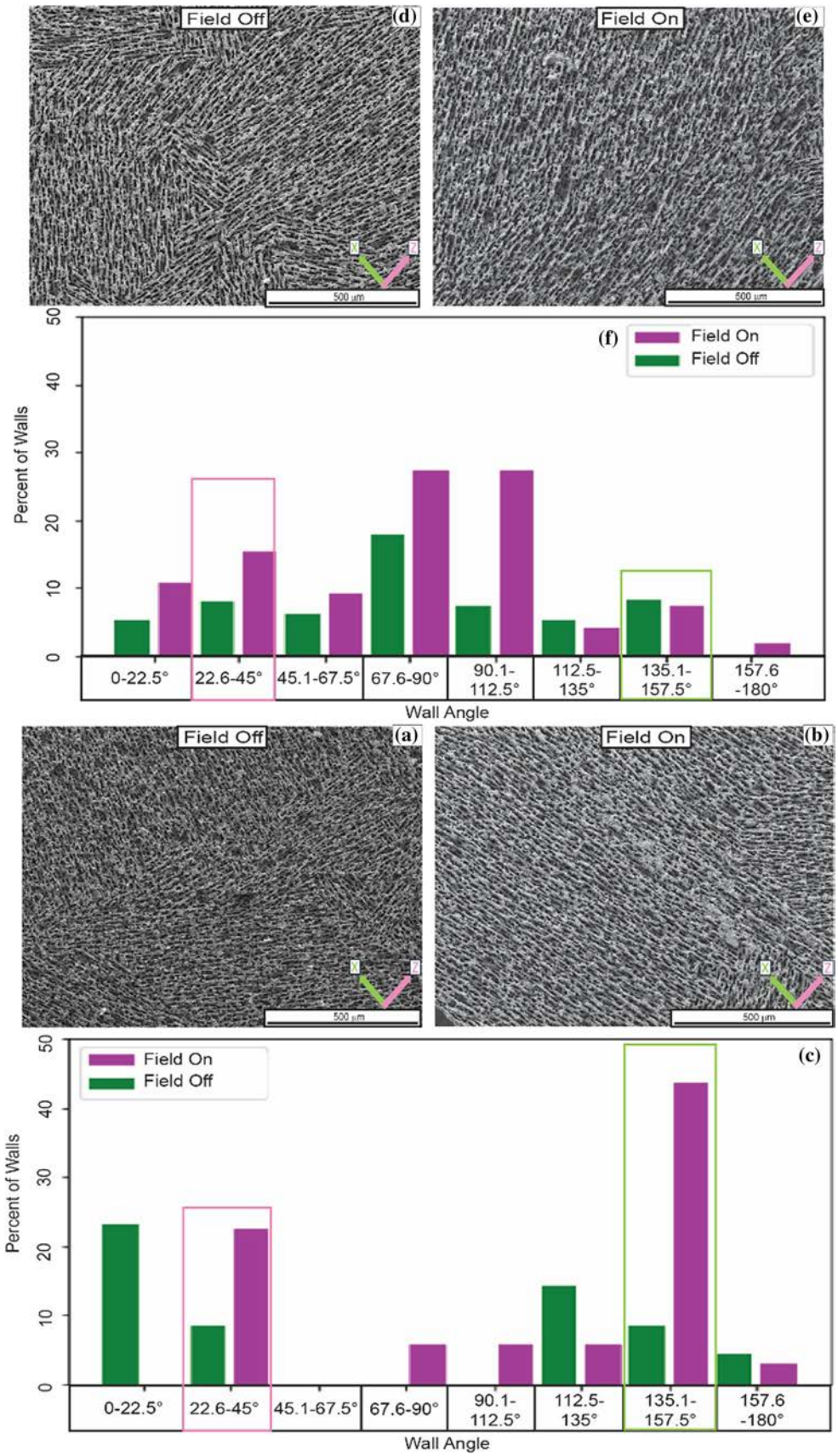

Figure 11 Scanning electron microscopy (SEM) images of surface-magnetized platelet scaffolds where no field was applied **a** and where a field was applied in the *x* direction (7.8mT) **b**. The corresponding change in wall alignment can be seen in the plot below **c**. Walls aligned in the *x* direction (green), which corresponds with the amount of alignment in seen in the *x* direction (green box) in the plot below **c.** The bar plot shows the percentage of walls in surface-magnetized platelet scaffolds that were in angle range. SEM image of mixed scaffold where no field was applied **d** and where the field was applied in the *x* direction (7.8mT) **e**. Walls are aligned in the *z* direction (pink), which corresponds with the amount of alignment in seen in the *z* direction (pink box) in the plot to the left **f**.

Conclusions

Per the study of scaffolds made using surface-magnetized alumina of differing aspect ratios created by magnetic freeze-casting, the following conclusions can be drawn:

(1) Magnetic freeze-casting with surface-magnetized particles of increased aspect ratio (platelets) creates scaffolds with improved UCS in all directions compared to scaffolds composed of just surface-magnetized particles.
(2) Greater wall alignment can be achieved in surface-magnetized platelet scaffolds compared to surface-magnetized particle scaffolds due to platelets having a greater magnetic moment than particles.
(3) Increased cross-bridging in surface-magnetized platelet scaffolds prevents an accompanying increase in UCS with the increase in alignment. Combining this with the overall increase in UCS could make alumina scaffolds better suited for a number of applications (dental implants, aerospace, medical devices, etc.).
(4) Applying a magnetic field in the x direction to mixed (1 platelets/1 particles) freeze-cast scaffolds increases the UCS_Z. Mixed scaffolds have a lower viscosity than platelet scaffolds, which enables the Hall effect to occur and causes the alignment seen in the z direction (perpendicular to the applied magnetic field). Thus, the Hall effect can be used to tailor the mechanical properties of surface-magnetized mixed scaffolds to better suit their uses.

Acknowledgements

This work was financially supported in part by the Army Research Office under grant W911NF-21-1-0062. The authors would like to acknowledge Orville Clarke for his expertise and contributions to this work.

Author contribution

MAS was responsible for experimental design, carrying out measurements, analyzing results, and composing the manuscript. SEN was responsible for conception and some experimental design. IN was responsible for capturing images used in the work.

Declarations

Conflict of interest The author declares no conflicts of interest or competing interests.

References

[1] Al-Sanabani FA, Madfa AA, Al-Qudaimi NH (2014) Alumina ceramic for dental applications: a review article. Am J Mater Res 1(1):26–34
[2] Zake-Tiluga I, Svinka V, Svinka R, Zierath B, Greil P, Fey T (2016) Thermal conductivity and microstructure characterisation of lightweight alumina and alumina–mullite ceramics. J Eur Ceram Soc 36:1469–1477. https://doi.org/10.1016/j.jeurceramsoc.2015.12.026
[3] Hunger PM, Donius AE, Wegst UGK (2013) Platelets self-assemble into porous nacre during freeze casting. J Mech Behav Biomed Mater 19:87–93. https://doi.org/10.1016/j.jmbbm.2012.10.013
[4] Munro M (1997) Evaluated material properties for a sintered alpha-alumina. J Am Ceram Soc 80:1919–1928. https://doi.org/10.1111/j.1151-2916.1997.tb03074.x
[5] Auerkari P (1996) Mechanical and physical properties of engineering alumina ceramics, Vol. 23. Espoo: Technical Research Centre of Finland
[6] Macdonald N, Bankes M (2014) Ceramic on ceramic hip prostheses: a review of past and modern materials. Arch Orthop Trauma Surg 134:1325–1333. https://doi.org/10.1007/s00402-014-2020-x
[7] Ishikawa K, Matsuya S, Miyamoto Y, Kawate K (2003) 9.05 - Bioceramics, in: I. Milne, R.O. Ritchie, B. Karihaloo (Eds.), Comprehensive Structural Integrity, Pergamon, Oxford, 2003: pp. 169–214. https://doi.org/10.1016/B0-08-043749-4/09146-1
[8] Yoon B-H, Choi W-Y, Kim H-E, Kim J-H, Koh Y-H (2008) Aligned porous alumina ceramics with high compressive strengths for bone tissue engineering. Scripta Mater 58:537–540. https://doi.org/10.1016/j.scriptamat.2007.11.006
[9] Koli DK, Agnihotri G, Purohit R (2015) Advanced aluminium matrix composites: the critical need of automotive and aerospace engineering fields. Mater Today Proceed 2:3032–3041. https://doi.org/10.1016/j.matpr.2015.07.290

[10] Deville S (2010) Freeze-casting of porous biomaterials: structure properties and opportunities. Materials 3:1913–1927. https://doi.org/10.3390/ma3031913

[11] Porter MM, Yeh M, Strawson J, Goehring T, Lujan S, Siripasopsotorn P, Meyers MA, McKittrick J (2012) Magnetic freeze casting inspired by nature. Mater Sci Eng, A 556:741–750. https://doi.org/10.1016/j.msea.2012.07.058

[12] Porter MM, McKittrick J, Meyers MA (2023) Biomimetic materials by freeze casting | SpringerLink, (2013). https://link.springer.com/article/https://doi.org/10.1007/s11837-013-0606-3 (accessed February 20, 2023)

[13] Sabat S, Sikder S, Behera SK, Paul A (2021) Effect of freezing velocity and platelet size on structural parameters and morphology of freeze-cast porous alumina scaffolds. Ceram Int 47:16661–16673. https://doi.org/10.1016/j.ceramint.2021.02.237

[14] Korber C, Rau G, Cosman M, Cravalho E (1985) Interaction of particles and a moving ice-liquid interface. J Cryst Growth 72:649–662. https://doi.org/10.1016/0022-0248(85)90217-9

[15] Deville S, Saiz E, Tomsia AP (2006) Freeze casting of hydroxyapatite scaffolds for bone tissue engineering. Biomaterials 27:5480–5489. https://doi.org/10.1016/j.biomaterials.2006.06.028

[16] Frank MB, Hei Siu S, Karandikar K, Liu C-H, Naleway SE, Porter MM, Graeve OA, McKittrick J (2017) Synergistic structures from magnetic freeze casting with surface magnetized alumina particles and platelets. J Mech Behav Biomed Mater 76:153–163. https://doi.org/10.1016/j.jmbbm.2017.06.002

[17] Frank MB, Naleway SE, Haroush T, Liu C-H, Siu SH, Ng J, Torres I, Ismail A, Karandikar K, Porter MM, Graeve OA, McKittrick J (2017) Stiff, porous scaffolds from magnetized alumina particles aligned by magnetic freeze casting. Mater Sci Eng C 77:484–492. https://doi.org/10.1016/j.msec.2017.03.246

[18] Nelson I, Naleway SE (2019) Intrinsic and extrinsic control of freeze casting. J Market Res 8:2372–2385. https://doi.org/10.1016/j.jmrt.2018.11.011

[19] Mroz M, Rosenberg JL, Acevedo C, Kruzic JJ, Raeymaekers B, Naleway SE (2020) Ultrasound freeze-casting of a biomimetic layered microstructure in epoxy-ceramic composite materials to increase strength and hardness. Materialia 12:100754. https://doi.org/10.1016/j.mtla.2020.100754

[20] Chi J, Wang M, Chen J, Hu L, Chen Z, Backman LJ, Zhang W (2022) Topographic orientation of scaffolds for tissue regeneration: recent advances in biomaterial design and applications. Biomimetics 7:131. https://doi.org/10.3390/biomimetics7030131

[21] Zhang Y, Hu L, Han J (2009) Preparation of a dense/porous bilayered ceramic by applying an electric field during freeze casting. J Am Ceram Soc 92:1874–1876. https://doi.org/10.1111/j.1551-2916.2009.03110.x

[22] Niksiar P, Su FY, Frank MB, Ogden TA, Naleway SE, Meyers MA, McKittrick J, Porter MM (2019) External field assisted freeze casting. Ceramics 2:208–234. https://doi.org/10.3390/ceramics2010018

[23] Nelson I, Varga J, Wadsworth P, Mroz M, Kruzic JJ, Kingstedt OT, Naleway SE (2020) Helical and Bouligand porous scaffolds fabricated by dynamic low strength magnetic field freeze casting. JOM 72:1498–1508. https://doi.org/10.1007/s11837-019-04002-9

[24] Nelson I, Gardner L, Carlson K, Naleway SE (2019) Freeze casting of iron oxide subject to a tri-axial nested Helmholtz-coils driven uniform magnetic field for tailored porous scaffolds. Acta Mater 173:106–116. https://doi.org/10.1016/j.actamat.2019.05.003

[25] Gamboa G, Wright Z, Berman D, Aouadi S, Young ML, Ku N, Brennan RE (2023) Experimental investigation and simulation of Al/B4C metal matrix composites produced using magnetic field-assisted freeze-casting of porous ceramic structures. MRS Adv 8:59–65. https://doi.org/10.1557/s43580-023-00502-8

[26] Bakkar S, Thapliyal S, Ku N, Berman D, Aouadi SM, Brennan RE, Young ML (2022) Controlling anisotropy of porous B4C structures through magnetic field-assisted freeze-casting. Ceram Int 48:6750–6757. https://doi.org/10.1016/j.ceramint.2021.11.226

[27] Porter MM, Meraz L, Calderon A, Choi H, Chouhan A, Wang L, Meyers MA, McKittrick J (2015) Torsional properties of helix-reinforced composites fabricated by magnetic freeze casting. Compos Struct 119:174–184. https://doi.org/10.1016/j.compstruct.2014.08.033

[28] Nelson I, Ogden TA, Al Khateeb S, Graser J, Sparks TD, Abbott JJ, Naleway SE (2019) Freeze-casting of surface-magnetized iron(II, III) oxide particles in a uniform static magnetic field generated by a Helmholtz coil. Adv Eng Mater 21:1801092. https://doi.org/10.1002/adem.201801092

[29] Zijlstra H (1942) Chapter 2 Permanent magnets; theory In: Handbook of Ferromagnetic Materials, Elsevier, 1982: pp. 37–105. https://doi.org/10.1016/S1574-9304(05)80088-4

[30] Jang S-M, Park H-I, Choi J-Y, Ko K-J, Lee S-H (2011) Magnet pole shape design of permanent magnet machine for minimization of torque ripple based on electromagnetic

field theory. IEEE Trans Magn 47:3586–3589. https://doi.org/10.1109/TMAG.2011.2151846

[31] Yong-Zhou H (2013) Inhomogeneity of external magnetic field for permanent magnet. Acta Phys Sin 62:084105. https://doi.org/10.7498/aps.62.084105

[32] Porter MM, Niksiar P, McKittrick J (2016) Microstructural control of colloidal-based ceramics by directional solidification under weak magnetic fields. J Am Ceram Soc 99:1917–1926. https://doi.org/10.1111/jace.14183

[33] Fernquist JR, Fu HC, Naleway SE (2022) Improved structural and mechanical performance of iron oxide scaffolds freeze cast under oscillating magnetic fields. Ceram Int 48:15034–15042. https://doi.org/10.1016/j.ceramint.2022.02.032

[34] Abbott JJ (2015) Parametric design of tri-axial nested Helmholtz coils. Rev Sci Instrum 86:054701. https://doi.org/10.1063/1.4919400

[35] Erb RM, Libanori R, Rothfuchs N, Studart AR (2012) Composites reinforced in three dimensions by using low magnetic fields. Science 335:199–204. https://doi.org/10.1126/science.1210822

[36] Libanori R, Erb RM, Studart AR (2013) Mechanics of platelet-reinforced composites assembled using mechanical and magnetic stimuli. ACS Appl Mater Interfaces 5:10794–10805. https://doi.org/10.1021/am402975a

[37] Bakkar S, Lee J, Ku N, Berman D, Aouadi SM, Brennan RE, Young ML (2020) Design of porous aluminum oxide ceramics using magnetic field-assisted freeze-casting. J Mater Res 35:2859–2869. https://doi.org/10.1557/jmr.2020.197

[38] Young HD, Freedman RA (2015) University Physics with Modern Physics (14th Edition), Pearson, Upper Saddle River, Nj, USA, 2015. https://www.biblio.com/book/university-physics-modern-physics-14th-edition/d/1342642250 (Accessed May 22, 2023)

[39] Ghosh D, Banda M, Kang H, Dhavale N (2016) Platelets-induced stiffening and strengthening of ice-templated highly porous alumina scaffolds. Scripta Mater 125:29–33. https://doi.org/10.1016/j.scriptamat.2016.07.030

[40] Ghosh D, Banda M, John JE, Terrones DA (2018) Dynamic strength enhancement and strain rate sensitivity in ice-templated ceramics processed with and without anisometric particles. Scripta Mater 154:236–240. https://doi.org/10.1016/j.scriptamat.2018.06.006

[41] Hunger PM, Donius AE, Wegst UGK (2013) Structure–property-processing correlations in freeze-cast composite scaffolds. Acta Biomater 9:6338–6348. https://doi.org/10.1016/j.actbio.2013.01.012

[42] Scotti KL, Dunand DC (2018) Freeze casting–A review of processing, microstructure and properties via the open data repository FreezeCastingnet. Progr Mater Sci 94:243–305. https://doi.org/10.1016/j.pmatsci.2018.01.001

[43] Yin K, Reese BA, Sullivan CR, Wegst UGK (2021) Superior mechanical and magnetic performance of highly anisotropic sendust-flake composites freeze cast in a uniform magnetic field. Adv Func Mater 31:2007743. https://doi.org/10.1002/adfm.202007743

[44] Weaver JS, Kalidindi SR, Wegst UGK (2017) Structure-processing correlations and mechanical properties in freeze-cast Ti-6Al-4V with highly aligned porosity and a lightweight Ti-6Al-4V-PMMA composite with excellent energy absorption capability. Acta Mater 132:182–192. https://doi.org/10.1016/j.actamat.2017.02.031

[45] Ghosh D, Kang H, Banda M, Kamaha V (2017) Influence of anisotropic grains (platelets) on the microstructure and uniaxial compressive response of ice-templated sintered alumina scaffolds. Acta Mater 125:1–14. https://doi.org/10.1016/j.actamat.2016.11.047

[46] Munch E, Saiz E, Tomsia AP, Deville S (2009) Architectural control of freeze-cast ceramics through additives and templating. J Am Ceram Soc 92:1534–1539. https://doi.org/10.1111/j.1551-2916.2009.03087.x

[47] Karplus R, Luttinger JM (1954) Hall effect in ferromagnetics. Phys Rev 95:1154–1160. https://doi.org/10.1103/PhysRev.95.1154

[48] Luckham PF, Ukeje MA (1999) Effect of particle size distribution on the rheology of dispersed systems | Elsevier Enhanced Reader. https://doi.org/10.1006/jcis.1999.6515

[49] Joukhdar H, Seifert A, Jüngst T, Groll J, Lord MS, Rnjak-Kovacina J (2021) Ice templating soft matter: fundamental principles and fabrication approaches to tailor pore structure and morphology and their biomedical applications. Adv Mater 33:2100091. https://doi.org/10.1002/adma.202100091

[50] Asha SK, Sunitha G (2020) Thermal radiation and Hall effects on peristaltic blood flow with double diffusion in the presence of nanoparticles. Case Stud Thermal Eng 17:100560. https://doi.org/10.1016/j.csite.2019.100560

[51] Ramsden E (2011) Hall-Effect Sensors: Theory and Application, Elsevier

[52] Caldas AMA, Caldas AGA, Dos Santos CAC, Ochoa AAV, Cézar KL, Michima PSA (2020) Design, development and construction of Hall effect-based turbine meter type to measure flow in low-cost lithium bromide salt: Proposed flowmeter and first results. Int J Refrig 112:240–250. https://doi.org/10.1016/j.ijrefrig.2020.01.002